

**Original citation:**

Chatterjee, Sourav, Houlding, Thomas K., Doluda, Valentin Yu., Molchanov, Vladimir P., Matveeva, Valentina G. and Rebrov, Evgeny V.. (2017) Thermal behavior of a catalytic packed-Bed Milli-reactor operated under radio frequency heating. *Industrial & Engineering Chemistry Research*.

**Permanent WRAP URL:**

<http://wrap.warwick.ac.uk/94495>

**Copyright and reuse:**

The Warwick Research Archive Portal (WRAP) makes this work by researchers of the University of Warwick available open access under the following conditions. Copyright © and all moral rights to the version of the paper presented here belong to the individual author(s) and/or other copyright owners. To the extent reasonable and practicable the material made available in WRAP has been checked for eligibility before being made available.

Copies of full items can be used for personal research or study, educational, or not-for profit purposes without prior permission or charge. Provided that the authors, title and full bibliographic details are credited, a hyperlink and/or URL is given for the original metadata page and the content is not changed in any way.

**Publisher's statement:**

"This document is the Accepted Manuscript version of a Published Work that appeared in final form in *Industrial & Engineering Chemistry Research*. copyright © American Chemical Society after peer review and technical editing by the publisher.

To access the final edited and published work

<http://pubs.acs.org/page/policy/articlesonrequest/index.html> ."

**A note on versions:**

The version presented here may differ from the published version or, version of record, if you wish to cite this item you are advised to consult the publisher's version. Please see the 'permanent WRAP URL above for details on accessing the published version and note that access may require a subscription.

For more information, please contact the WRAP Team at: [wrap@warwick.ac.uk](mailto:wrap@warwick.ac.uk)

# **Thermal behavior of a catalytic packed-bed milli-reactor operated under radiofrequency heating**

Sourav Chatterjee<sup>1</sup>, Thomas K. Houlding<sup>1</sup>, Valentin Yu. Doluda<sup>2</sup>, Vladimir P. Molchanov<sup>2</sup>

Valentina G. Matveeva<sup>2</sup>, Evgeny V. Rebrov<sup>2,3\*</sup>

<sup>1</sup> School of Chemistry & Chemical Engineering, Queen's University Belfast, Stranmillis Road, BT9 5AG, Belfast, UK

<sup>2</sup> Department of Biotechnology and Chemistry, Tver State Technical University, 170026, Tver Russia

<sup>3</sup> School of Engineering, University of Warwick, CV4 7AL Coventry, UK

\*Corresponding author: [e.rebrov@warwick.ac.uk](mailto:e.rebrov@warwick.ac.uk)

## **Abstract**

An approach for analysis of thermal gradients in a catalytic packed bed milli-reactor operated under radiofrequency (RF) heating has been presented. A single-point temperature measurement would cause the misinterpretation of the catalytic activity in an RF-heated reactor due to the presence of a temperature gradient. For reliable data interpretation, the temperature should be measured at three positions along the reactor length. The temperature profile can be accurately estimated with the exact analytical solution of a 1D convection and conduction heat-transfer model and it can also be approximated with a second-order polynomial function. The results revealed that the position of maximum temperature in the catalytic bed shifts towards a downstream location as the flow rate increases. The relative contribution of conduction and

convection to the overall heat transport has been discussed. The design criteria for a near isothermal milli-reactor have been suggested.

## 1. Introduction

The fact that small-scale and distributed chemical manufacturing systems are proved to offer advantages such as lower capital and operating expenses, compactness of equipment, relatively small energy consumption and reduced by-product formation<sup>1-4</sup> has led to the growing interest in newer process intensification methods using reactors with channel diameter in the millimeter range (milli-reactors)<sup>5-8</sup>. Among them, radiofrequency heating (RF) plays an important role to enhance the rate of catalytic reactions<sup>9-12</sup>. In this method, the energy is provided to the reactor by an alternating magnetic field in the 100-1000 kHz range. The application of RF heating requires to use composite magnetic catalysts composed of a magnetic material and an active catalyst or an adsorbent<sup>13</sup>. RF induced desorption from composite pellets have been recently demonstrated<sup>14</sup>.

Catalytic packed bed reactors are the most extensively employed reactor type for laboratory and small scale chemical production<sup>15,16</sup>. In general, this kind of reactors involves mass of catalyst ranging from 10 to 500 mg and volumetric flow rates up to 10 mL min<sup>-1</sup>. There are no qualitative criteria for the existence of substantial temperature gradients in the flow direction as a result of volumetric heating and heat transfer. For many chemical processes in tubular reactors, a temperature gradient can improve the conversion as much higher reaction rate can be achieved towards the end zone maintained at higher temperature. For example, in an endothermic equilibrium limited reaction, such as methanol steam reforming, a thermal gradient offers the possibility of substantially increasing the conversion as compared to that in an isothermal or adiabatic process<sup>17</sup>. However there are also applications where even a small deviation of the catalyst temperature from an isothermal operation would result in a substantial decrease of selectivity. Those are partial oxidation and preferential oxidation reaction, just to mention a few<sup>18</sup>.

In the absence of convective flux, the general empirical rule to avoid temperature non-uniformity is that the conductive thermal resistance in the solid bed,  $R_A$ , (Eq. 1) should be much smaller as compared to the combined thermal resistance of the reactor wall ( $R_{B1}$ ), insulation ( $R_{B2}$ ), and natural convection ( $R_{B3}$ , Eq. 2):  $R_A \ll R_B$ ,

$$R_A = \frac{L}{\lambda_1 A_\perp} \quad (1)$$

$$R_B = R_{B1} + R_{B2} + R_{B3} = \frac{\ln\left(\frac{r_2}{r_1}\right)}{2\pi L \lambda_2} + \frac{\ln\left(\frac{r_3}{r_2}\right)}{2\pi L \lambda_3} + \frac{1}{h_3 A_3} \quad (2)$$

where  $r_1$  is the inner radius of reactor,  $r_2$  is the outer radius of reactor,  $r_3$  is the outer radius of insulation,  $\lambda_1$  is the effective thermal conductivity of the catalyst bed,  $\lambda_2$  is the thermal conductivity of the reactor wall,  $\lambda_3$  is the thermal conductivity of insulation,  $L$  is the length of reactor,  $h_3$  is the natural convection heat transfer coefficient,  $A_\perp$  is the cross sectional area of the reactor and  $A_3$  is the external surface area of insulation.

However in the presence of liquid flow, the thermal analysis becomes more complex. Modelling heat transfer in mini- and micro-devices requires taking convective heat transfer into account. Disregarding this effect can lead to very large bias in the experimental estimation of heat transfer contributions, especially for larger Reynolds numbers. As a result of convective heat flux, the position of maximum temperature under volumetric heating shifts from the central part of the reactor towards a downstream location<sup>19</sup>. Tiselj et al. studied the effect of axial heat flux on heat transfer in microchannels at Re numbers in the range between 3 and 160<sup>20</sup>. The authors experimentally determined the axial heat flux values to verify their numerical calculations performed with a model which included a silicon chip with seventeen parallel microchannels with a length of 15 mm. The axial position corresponding to the maximum temperature in a microchannel shifts towards the channel outlet with an increase in

the flow rate<sup>20</sup>. Patil et al.<sup>21</sup> reported that the position of the maximum temperature shifts towards the outlet with a decrease in the volumetric heat generation power.

To evaluate the effect of axial heat conduction, Maranzana et al.<sup>22</sup> proposed a quantifying factor ( $M$ , Eq. 3) which is the ratio between axial heat transfer by conduction in the wall ( $\Phi_{cond}$ ) and convective heat transfer in the flow ( $\Phi_{conv}$ ).

$$M = \frac{\Phi_{cond}}{\Phi_{conv}} = \frac{1/R_A}{\rho C_p F_V} \quad (3)$$

where  $F_V$  is the volumetric flow rate,  $\rho$  is the density of fluid,  $C_p$  is the specific heat capacity of fluid. They concluded that with high  $M$  factor, which states that axial heat conduction is the main mechanism of heat transfer, the fluid temperature profile in the channel became non-linear and heat flux at channel entrance increases as compared to the classical theory<sup>22</sup>. Huang et al.<sup>23</sup> confirmed experimentally that at higher  $M$  factors, much stronger temperature gradient develops in the first section of channel as compared to the case of low  $M$  values. The axial heat flux is typically larger than the radial heat flux<sup>19,24</sup>. Still the both contributions should be taken into account due to much larger area for radial heat exchange in micro- and milli-reactors. The radial heat losses can be reduced by insulation or temperature compensation, both reducing driving force for heat transfer<sup>25</sup>.

A large number of contributions in literature are devoted to simulations of the complete behavior of a flow reactor, formulating and solving the momentum, mass and energy conservation balances<sup>26,27</sup>. In that way, Qu and Mudawar<sup>28,29</sup> performed numerical simulations of heat transfer in a single phase microchannel by solving the conjugate heat transfer problem involving simultaneous determination of the temperature field in both solid and fluid regions. They compared the numerical results with experimental data and showed good agreement between the local fluid and wall temperatures at different locations along the channel. Such an approach allows a proper analysis of the experimental results, even if some significant departure from the isothermal behavior occurs. Although three-dimensional conjugate heat

transfer analyses of catalytic microchannels was shown to provide satisfactory results as compared with the experimental measurements, they are computationally expensive, case-specific and cannot be generalized to a wide range of reactor configurations.

The goal of this work was to develop a simplified approach to predict temperature profiles in an RF-heated flow milli-channel reactor. To achieve this goal, two different approaches were employed. In the first approach, an analytical solution was used to estimate temperature profiles in the milli-channel reactor based on an energy balance. These results were compared with the exact solution obtained by a 3D convection and conduction model which represents the second approach. The model accounted for the effect of hydrodynamic and thermal developing boundary layers on the pressure drop and heat transfer.

## **2. Materials and methods**

A quartz reactor (45 mm length, i.d. 4 mm, o.d. 6 mm) was split into three zones. The middle section with a length of 25 mm consisted of composite magnetic catalyst (CMC) pellets (125-250  $\mu\text{m}$ ) that generated heat under RF field. The details of preparation of the magnetic catalyst and CMC pellets are reported elsewhere<sup>13</sup>. A schematic view of the central reactor section is shown in Figure 1.

Insert Figure 1 here

The two adjacent sections with a length of 10 mm were filled with inert pellets of the same size and thermal properties as those in the middle section while those sections were not heated by RF field. This allowed creating the same hydrodynamic conditions in all three sections. The reactor was placed inside an RF coil with a diameter of 46 mm connected to an Easyheat system, generating a uniform RF field inside the coil at a frequency of 280 kHz. Cooling water

was supplied by a Lauda thermostat and was circulated through the coil during operation. Three fiber optic temperature sensors (Opsens) were attached to the exterior of the reactor at positions  $x_A = 5.0$  mm,  $x_B = 12$  mm and  $x_C = 20$  mm along the axial coordinate, measuring temperatures  $T_A$ ,  $T_B$  and  $T_C$  respectively. The accuracy of the fiber optic sensors is 0.1 K. The reactor dimensions and material thermal properties are listed in Table 1 and shown in Figure 1.

Insert Table 1 here.

The amount of heat generated by the composite material ( $q$ ) was determined from the heat balance in a non-reacting system. The RF power level was controlled to obtain the required temperature at any specific flow rate. Para-xylene (99.5 wt. %, Fluka) was fed to the reactor by a Shimadzu LC-20AD HPLC pump with a flow rate in the range between 0 and 200  $\mu\text{L min}^{-1}$ . The system was pressurized to 7 bar using an Upchurch P-787 PEEK backpressure regulator to avoid evaporation of xylene. To study a catalytic reaction of direct amide synthesis from an amine and a carboxylic acid, two HPLC pumps were used to feed solutions of aniline and 4-phenylbutyric acid. The product analysis was performed with a Shimadzu GC-2010 gas chromatograph equipped with a 30 m Staliwax capillary column and an FID detector. Carbon balance was 99.5 % in all experiments.

### 3. Results and discussion

The conductive thermal resistance of the catalyst bed ( $R_A$ ) is calculated by Eq. 1. The obtained value of 590  $\text{K W}^{-1}$  is larger than that of  $R_B$  (Eq. 2) of 330  $\text{K W}^{-1}$ . This means that there is a temperature gradient in the reactor under volumetric heating even in the absence of fluid flow. The  $M$  value, obtained by Eq. 3, is 0.43 indicates a considerable contribution by convection which eventually results in a non-symmetrical thermal gradient in the axial direction.



The value for the overall heat transfer coefficient ( $U$ ) of the composite wall was determined from the combined thermal resistance,  $R_B$

$$U = \frac{1}{R_B A} \quad (4)$$

The effective thermal conductivity ( $\lambda_1$ ) of the catalyst bed depends on the bed porosity. Typical values between  $4 \text{ W m}^{-1} \text{ K}^{-1}$ <sup>27</sup> and  $12 \text{ W m}^{-1} \text{ K}^{-1}$ <sup>28</sup> are reported. In the current study, a value of  $6.7 \text{ W m}^{-1} \text{ K}^{-1}$  was obtained from a transient experiment. In this experiment, the temperature of the bed has been measured by fast heating of a part of the magnetic bed section inside the RF coil by 50 K (within 1 s) while keeping other part of the bed at room temperature (outside the coil). Then following the temperature distribution in the bed at different times, the effective thermal conductivity of the bed was calculated.

Two methods were employed to obtain temperature profiles: (1) an analytical solution to a 1D heat transfer model including volumetric heat generation and convective flux; (2) a numerical solution to a 1D heat transfer model including axial dispersion and the effect of hydrodynamic and thermal developing boundary layers in the entrance region.

### *3.1 Temperature profile in the reactor*

The conventional method for kinetic analysis involves independent variation of temperature and flow rate to obtain a set of kinetic data. In the first approach, the temperatures were measured at three axial positions at several flow rates and the temperature profiles were approximated with a second order polynomial function (Figure 2). A significant temperature gradient occurs within the reactor under volumetric heating which is in line with the assumption based on comparison of  $R_A$  and  $R_B$  values. Therefore any approach based on a single temperature measurement would be invalid.

Insert Figure 2 here

Under RF field, the shape of the temperature profile depends both on the power input and flow rate. At a constant power input of 3.1 W, the average temperature decreases from 181 to 124 °C as the flow rate increases from 40 to 200  $\mu\text{l min}^{-1}$  (Figure 2a). In addition, the position of the maximum temperature gradually shifts downstream as the flow rate increases. At the highest flow rate of 200  $\mu\text{l min}^{-1}$ , the highest temperature is observed at a distance  $x^* = 0.77$ . In the absence of the fluid flow, the temperature profile becomes symmetrical relative to the center of the bed. As the power input increases from 2.7 to 3.8 W at a constant flow rate of 160  $\mu\text{l min}^{-1}$ , the average temperature increases from 112 to 181 °C while the degree of concavity of temperature profiles remains almost the same (Figure 2b).

A one dimensional (1D) pseudo-homogeneous dispersed plug flow model can be employed to formulate the energy balance within the heating zone:

$$k_{eff} \frac{d^2T}{dx^2} - GC_p \frac{dT}{dx} - \frac{4}{d_h} U(T - T_{env}) + q_{av} = 0 \quad (5)$$

where  $q_{av}$  is the volumetric heat generation rate in the reactor. The volumetric heat generation rate was calculated from the intensity of magnetic field and the efficiency of conversion of electromagnetic energy into heat and it was verified from the heat balance in the absence of fluid flow. The efficiency of conversion of RF field into heat is 84% in the RF coil. The intensity of electromagnetic field along both radial and axial dimensions is rather uniform. This is because the reactor diameter (4 mm) is considerably smaller than the coil diameter (46 mm) and the bed length is smaller than the coil length. This provides very uniform magnetic field and volumetric energy supply along both radial and axial dimensions.

The heat transfer rate depends on two effective thermal parameters: the overall heat transfer coefficient  $U$  between the bed and the environment, and the effective axial thermal conductivity,  $k_{eff}$ . Eq. 5 describes the  $T(x^*)$  profile of the temperature averaged over the cross

section of the reactor. The boundary conditions are chosen such that the temperature far away from the heating zone reaches the temperature of the environment:  $T(-\infty) = T(\infty) = T_{env}$ . The solution of Eq. 5 can be presented in a form:

$$T - T_{env} = \frac{q_{av} d_h}{4U} \left[ 1 - \frac{z_2}{z_1 + z_2} e^{-z_1(1-x^*)} - \frac{z_1}{z_1 + z_2} e^{-z_2 x^*} \right] \quad (6)$$

where  $z_1$  and  $-z_2$  are the characteristic roots which can be expressed as follows:

$$z_1 = 2L \sqrt{\frac{U}{d_h \lambda_{eff}}} \cdot \left[ \frac{R_C}{2} + \sqrt{1 + \frac{R_C^2}{4}} \right] \quad (7a)$$

$$z_2 = \frac{2L \sqrt{\frac{U}{d_h \lambda_{eff}}}}{\frac{R_C}{2} + \sqrt{1 + \frac{R_C^2}{4}}} \quad (7b)$$

$$R_C^2 = \frac{d_h (GC_p)^2}{4 \lambda_{eff} U} \quad (7c)$$

The temperature gradient depends on the dimensionless parameter,  $R_C$ , describing the ratio between the effect of heat convection and that of axial heat dispersion. At very low flow rate,  $R_C \ll 1$ , and the effect of convection heat transfer can be neglected. The solution becomes

$$z_0 = z_1 = z_2 = 2L \sqrt{\frac{U}{d_h \lambda_{eff}}} \quad (8)$$

The position of the maximum in the temperature profile can be determined from condition

$\frac{dT}{dx} = 0$ . Taking the first derivative of Eq. 6 and equalizing it to zero, one would obtain:

$$\frac{-z_1 z_2}{z_1 + z_2} e^{-z_1} e^{z_1 x_{MAX}^*} + \frac{z_1 z_2}{z_1 + z_2} e^{-z_2 x_{MAX}^*} = 0 \quad (9)$$

Solving Eq. 9 for the position of the maximum, one would obtain:

$$x_{MAX}^* = \frac{z_1}{z_1 + z_2} \quad (10)$$

From this value, the maximum temperature can be evaluated from Eq. 6:

$$T_{\max} = T_{env} + \frac{q_{av}d_h}{4U} \left[ \frac{z_1}{z_1 + z_2} + \frac{z_2}{z_1 + z_2} e^{-z_1} - e^{-\frac{z_1 z_2}{z_1 + z_2}} \right] \quad (11)$$

The maximum temperature is a function of the overall heat transfer coefficient, the thickness of the insulation and the effective axial thermal conductivity of the catalyst. However at very low flow rate,  $R_C \ll 1$ , and  $z_1 = z_2 = z_0$ . In this case, Eq. 6 can be simplified to

$$T - T_{env} = \frac{q_{av}d_h}{8U} \left[ 2 - e^{-z_0(1-x^*)} - e^{-z_0x^*} \right] \quad (12)$$

The temperature profile is symmetrical relative  $x_{MAX}^* = 0.5$  and the maximum temperature becomes

$$T_{\max} = T_{env} + \frac{q_{av}d_h}{8U} \left[ 1 + e^{-z_0} - 2e^{-\frac{z_0}{2}} \right] \quad (13)$$

If  $z_0$  is small, Eq. 13 can be expanded in series up to the second order terms:

$$T_{\max} = T_{env} + \frac{q_{av}d_h}{8U} \left[ 1 + \left( 1 - z_0 + \frac{z_0^2}{2} \right) - 2 \cdot \left( 1 - \frac{z_0}{2} + \frac{z_0^2}{8} \right) \right] = T_{env} + \frac{q_{av}d_h}{8U} \frac{z_0^2}{4} \quad (14)$$

Inserting Eq.8 in to Eq. 14 one can get expression for the maximum temperature in an RF heated reactor

$$T_{\max} = T_{env} + \frac{q_{av}L^2}{8\lambda_{eff}} \quad (15)$$

It can be seen from Eq. 15 that in this case, the maximum temperature does not depend on the overall heat transfer coefficient and the reactor diameter. The minimum temperature will be always at the reactor inlet:  $x_{MIN}^* = 0$ .

Making a new variable, the reactor half-length,  $l = \frac{L}{2}$ , the temperature profile becomes parabolic and symmetrical relative  $x=l$

$$T_{\max} - T_{env} = \frac{q_{av}}{2\lambda_{eff}} (x-l)^2 \quad (16)$$

We used both the exact (Eq. 6) and approximate (Eqs. 12 and 16) analytical solutions to predict the axial temperature profile and the maximum temperature difference at a constant volumetric heating rate. Eq. 6 predicts the maximum temperature rather well (Figure 3a). In the absence of convective flux, the profile is symmetrical and the maximum temperature is described by Eq. 15 rather well. From the energy balance, it is possible to estimate the contribution from the natural convection losses and therefore to estimate the overall heat transfer coefficient. The overall heat transfer coefficient (U) is equal to  $9.0 \text{ W m}^{-2}\text{K}^{-1}$ . A very close value of  $9.2 \text{ W m}^{-2}\text{K}^{-1}$  was obtained for  $h_3$  from a correlation for heat transfer rate around a horizontal cylinder (Eq. 17)<sup>30</sup>

$$Nu = \left[ 0.60 + \frac{0.387Ra^{0.16}}{\left[ 1 + \left( \frac{0.559}{Pr} \right)^{0.5625} \right]^{0.296}} \right]^2 \quad (17)$$

As the overall heat transfer coefficient is close to  $h_3$ , it can be concluded that the main heat transfer resistance is in the boundary layer around the insulation layer. In the flow experiments, the maximum position shifts to the downstream location. Again, the position of the maximum temperature is very well described by Eq. 6 (Figure 3b and Table 2).

Insert Table 2 here

A convection and conduction heat-transfer model was solved numerically in Comsol to verify the validity of the analytical solution (Figure 4). This model is essentially the same as previously presented<sup>31</sup> to estimate temperature profile in a trickle-bed reactor under RF heating.

The model was used to predict the temperature profiles in the reactor, using the same parameters as used for the analytical solution.

Insert Figure 4 here

The temperature profiles predicted by the numerical model were almost identical to those predicted by the analytical solution. The difference can be caused by axial dispersion effects in the numerical model which are not accounted in the analytical solution. Similar to the analytical solution, the maximum temperature was also observed to shift downstream for increasing flow rates.

### 3.2 Heat losses

Once an accurate description of temperature profiles in the reactor has been obtained, the overall heat balance can be estimated. While the description of temperature profiles given by Eq 6 is rather accurate, it is possible to replace the exact solution with a simple parabolic function as presented in Table 3.

Insert Table 3 here.

Such replacement allows to estimate the conductive heat loss at the both ends of the reactor using the Fourier's law of thermal conduction:

$$Q_{cond} = -\lambda_{eff} A_c \left( \left. \frac{dT}{dx^*} \right|_{x^*=0} + \left. \frac{dT}{dx^*} \right|_{x^*=1} \right) \quad (18)$$

using  $\lambda_{eff}$  of  $6.7 \text{ W m}^{-1} \cdot \text{K}^{-1}$  and the temperature gradient at the both ends of the reactor:  $\frac{dT}{dx^*}$  at  $x^*=0$  and  $x^*=1$ .

The heat losses to the environment were calculated by the Newton's law of cooling,

$$Q_{conv} = UA_s (\bar{T} - T_\infty) \quad (19)$$

where  $\bar{T}$  is the average temperature of the reactor bed over the length between  $x^*=0$  and  $x^*=1$ , and  $T_\infty$  is the temperature of the surrounding air which was set at 20 °C.

Finally the contribution of the fluid heating was estimated from the conservation of internal energy

$$Q_{heat} = F_V \rho C_p (T_1 - T_0) \quad (20)$$

where  $T_1$  and  $T_0$  is the mean temperature of the fluid leaving and entering the packed-bed, respectively. At steady-state conditions, the total heat transfer rate is equal to the heat generation via RF heating:

$$Q_{tot} = \dot{q} V = Q_{heat} + Q_{cond} + Q_{conv} \quad (21)$$

Figure 5 shows the contribution of different heat loss mechanisms in the reactor as a function of the flow rate.

Insert Figure 5 here

At flow rates below 200  $\mu\text{L min}^{-1}$ , conduction has the largest contribution to the overall heat loss (Figure 5). Conduction opposite to the flow direction plays a significant role in preheating the liquid before it enters the packed-bed. As the flow rate increases the contribution of both conduction and convection heat transfer decreases as a result of the decreased temperature gradient.

The position of the maximum temperature in the reactor can also be expressed as a function of M-factor (Eq. 3, Figure 6). Increasing the flow rate increases the contribution by forced convection and therefore the M factor decreases. In the region at  $M < 0.4$ , the maximum temperature positions shifts to the very end of the reactor, and at these conditions a major

amount of heat is transported away from the reactor by convection. This corresponds to  $R_C^2$  value above 3. At even larger values of  $R_C^2$ , the position of the maximum temperature would be located almost at the exit.

### *3.3. Recommendations for the choice of design parameter for RF-heated milli-reactor*

In case of a catalytic reaction taking place in the reactor, the heat transfer model should be coupled with an appropriate kinetic model either to predict the reactant concentration profiles or to estimate relevant kinetic parameters. While this can be done using modern CFD packages, such approach is rather time consuming and requires good initial guess values for fast convergence. However, the temperature profile under RF-heating can be rather good described by the analytical solution to a 1D heat transfer problem once the effective thermal conductivity of the bed and the overall heat transfer coefficient are known. Therefore an important simplifying step is the initial modelling of temperature profile from the known specific heat generation rate, which allows to decouple the energy conservation balance from the component mass balance. Finally, the obtained temperature profiles can be rather good described by a second order polynomial function which further simplifies the analysis.

It is however important in many applications that the maximum hot spot in the reactor should not exceed some critical value. On the other size, the experimental error due to the uncertainty of determination of overall heat transfer coefficient (U) should be reduced.

It has been shown that the exact value of  $T_{\max}$  can be estimated by Eq. 11 with high precision.

The maximum allowed magnitude of  $T_{\max}$  can be determined if the activation energy of reaction is known. In our past experiments, a temperature difference as low as 2 K can be maintained in the RF-heated reactor<sup>31,32</sup>. It can be seen from Eq. 15 that the temperature gradient increases as a second power of the reactor length. Therefore it is of importance that



the length to diameter ratio should be kept as low as possible to create near-isothermal conditions in the reactor. Also the M-value should be chosen below 1 to reduce the contribution from natural convection. However, the range of experimental flow rates is usually determined by the catalyst volume, so it is not always possible to increase the flow rate to decrease the M-value. While dilution of the magnetic catalyst will reduce the specific heat generation rate, this will increase the size of the total catalyst bed, and the overall effect will be much lower than expected. Therefore, an alternative approach can be used where a single catalytic bed can be split in several heating sections with additional sections of inert material in between<sup>32</sup>. In case of a non-magnetic catalyst, one catalytic and one heating zone form a single periodic unit which, in principle, can be repeated in the axial direction if the intensity of RF field in the axial direction remains the same. Further adjustments can be made by varying the position and the length of individual heating zones.

The importance of accurate temperature measurements is crucial for a proper interpretation of the catalytic activity in an RF heated reactor. Figure 7 compares two reactant concentration profiles simulated based on the kinetics of amide synthesis from of aniline and 4-phenylbutyric acid<sup>33</sup> and respective temperature distributions. The reaction follows a first order kinetics with respect to both reactants with a reaction rate of  $0.15 \mu\text{mol g}^{-1} \text{s}^{-1}$  at  $150 \text{ }^\circ\text{C}$  and an activation energy of  $48 \text{ kJ mol}^{-1}$  (Figure 8).

Figure 7a shows both temperature and amine concentration profiles under RF heating. A conversion of  $82.0 \pm 0.3\%$  was observed and the average temperature in the bed was  $181 \text{ }^\circ\text{C}$ . However if the same reactor was placed in a convection oven maintained at a constant temperature of  $181 \text{ }^\circ\text{C}$  over the entire reactor length, the conversion was  $78.8 \pm 0.3\%$  (Figure 7b). Thus, a single-point temperature measurement would cause the misinterpretation of the catalytic activity in an RF-heated reactor due to an underestimation of reaction rate. The difference is caused by much higher reaction rate in the central part of the catalytic bed under

RF heating. In other words, the temperature rise along the RF heated reactor length helps to keep high reaction rate in the downstream section of the reactor. Depending on the position of the fiber optic sensor and the fluid flow rate the difference between the single point kinetic model predictions and experimental data could be as high as 20% (Figure 9).

Insert Figures 7-9 here.

#### **4. Conclusions**

Determination of the temperature profile in an RF heated catalytic packed-bed milli-reactors is essential for interpretation of kinetic data in these systems. Due to their small dimensions larger contributions of axial conduction and heat losses to the environment are observed and accordingly the temperature profiles deviate from those observed in large scale reactors that follow adiabatic operation. The accurate determination of effective thermal conductivity is necessary for the estimation of the maximum temperature in the reactor and the position of this maximum. Therefore the temperature has to be measured at least at three different positions along the bed. This allows to determine the effective thermal conductivity from the exact analytical solution to a 1D convective and conduction heat transfer problem with internal heat generation. The M-factor (as suggested by Maranzana et al.<sup>22</sup>) should be below 0.4 to reduce the contribution from natural convection heat transfer and increase the accuracy of kinetic measurements. However once the M-factor exceeds 0.4, the axial conduction becomes the dominant mechanism of heat transfer and a more rigorous approach utilising numerical modelling has to be employed.

#### **Acknowledgement**

The financial support provided by the European Research Council t (project 279867, “RF-enhanced microprocessing for fine chemicals synthesis using catalysts supported on magnetic

nanoparticles, RFMiFiCS”), and the Russian Science Foundation (project 15-13-20015) is gratefully acknowledged.

## Literature Cited

- (1) Roberge, D.M.; Ducry, L.; Bieler, N.; Cretton, P.; Zimmermann, B. Microreactor Technology: A Revolution for the Fine Chemical and Pharmaceutical Industries? *Chem. Eng. Tech.* **2005**, *28*, 318.
- (2) Roberge, D.M.; Zimmermann, B.; Rainone, F.; Gottsponer, M.; Eyholzer, M.; Kockmann, N. Microreactor Technology and Continuous Processes in the Fine Chemical and Pharmaceutical Industry: Is the Revolution Underway? *Org. Proc. Res. Dev.* **2008**, *12*, 905.
- (3) Wiles, C.; Watts, P. Recent Advances in Micro Reaction Technology, *Chem. Comm.* **2011**, *47*, 6512.
- (4) Elvira, K.S.; Casadevall i Solvas, X.; Wootton, R.C.; de Mello A.J. The Past, Present and Potential for Microfluidic Reactor Technology in Chemical Synthesis, *Nature chemistry* **2013**, *5*, 905.
- (5) Hessel, V. Novel Process Windows – Gate to Maximizing Process Intensification via Flow Chemistry, *Chem. Eng. Tech.* **2009**, *32*, 1655.
- (6) Wegner, J.; Ceylan, S.; Kirschning, A. Ten Key Issues in Modern Flow Chemistry, *Chem. Comm.* **2011**, *47*, 4583.
- (7) Illg, T.; Löb, P.; Hessel, V. Flow Chemistry Using Milli- and Microstructured Reactors – from Conventional to Novel Process Windows, *Bioorg. Med. Chem.* **2010**, *18*, 3707.
- (8) Wegner, J.; Ceylan, S.; Kirschning, A. Flow Chemistry – A Key Enabling Technology for (Multistep) Organic Synthesis, *Adv. Synth. Catal.* **2012**, *354*, 17.
- (9) Ceylan, S.; Friese, C.; Lammel, C.; Mazac, K.; Kirschning, A. Inductive Heating for Organic Synthesis by Using Functionalized Magnetic Nanoparticles inside Microreactors, *Ang. Chem. Int. Ed.* **2008**, *47*, 8950.

- (10) Ceylan, S.; Coutable, L.; Wegner, J.; Kirschning, A. Inductive Heating with Magnetic Materials inside Flow Reactors, *Chemistry Europ. J.* **2011**, *17*, 1884.
- (11) Houlding, T.K.; Rebrov, E.V. Application of Alternative Energy Forms in Catalytic Reactor Engineering, *Green Proc.Synth.* **2012**, *1*, 19.
- (12) Latifi, M.; Berruti, F.; Briens, C. A Novel Fluidized and Induction Heated Microreactor for Catalyst Testing, *AIChE J.* **2014**, *60*, 3107.
- (13) Houlding, T.K.; Gao, P.; Degirmenci, V.; Tchabanenko, K.; Rebrov, E.V. Mechanochemical Synthesis of TiO<sub>2</sub>/NiFe<sub>2</sub>O<sub>4</sub> Magnetic Catalysts for Operation under RF Field, *Mater. Sci. Eng. B*, **2015**, *193*, 175.
- (14) Zadražil, A.; Štěpánek, F. Remote Control of Desorption by Radiofrequency Heating: Single Pellet Experiments, *Chem. Eng. Sci.* **2013**, *101*, 382.
- (15) Kirschning, A.; Solodenko, W.; Mennecke, K. Combining Enabling Techniques in Organic Synthesis: Continuous Flow Processes with heterogenized catalysts, *Chemistry Europ. J.* **2006**, *12*, 5972.
- (16) Frost, C.G.; Mutton, L. Heterogeneous Catalytic Synthesis Using Microreactor Technology, *Green Chem.* **2010**, *12*, 1687.
- (17) Chein, R.Y.; Chen, Y.C.; Chung, J.N. Axial Heat Conduction and Heat Supply Effects on Methanol-Steam Reforming Performance in Micro-Scale Reformers, *Int. J. Heat Mass Trans.* **2012**, *55*, 3029.
- (18) Snytnikov, P.V.; Popova, M.M.; Men, Y.; Rebrov, E.V.; Kolb, G.; Hessel, V.; Schouten, J.C.; Sobyenin, V.A. Preferential CO Oxidation over a Copper–Cerium Oxide Catalyst in a Microchannel Reactor, *Appl. Catal. A* **2008**, *350*, 53.
- (19) Rebrov, E.V.; Schouten, J.C.; De Croon, M.H.J.M. Single-Phase Fluid Flow Distribution and Heat Transfer in Microstructured Reactors, *Chem. Eng. Sci.* **2011**, *66*, 1374.

- (20) Tiselj, I.; Hetsroni, G.; Mavko, B.; Mosyak, A.; Pogrebnyak, E.; Segal, Z. Effect of Axial Conduction on the Heat Transfer in Micro-Channels, *Int. J. Heat Mass Trans.* **2004**, *47*, 2551.
- (21) Patil, N.G.; Rebrov, E.V.; Eränen, K.; Benaskar, F.; Meuldijk, J.; Mikkola, J.P.; Hessel, V.; Hulshof, L.A.; Murzin, D.Y.; Schouten, J.C. Effect of the Load Size on the Efficiency of Microwave Heating under Stop Flow and Continuous Flow Conditions, *J. Microwave Power E.E.* **2012**, *46*, 83.
- (22) Maranzana, G.; Perry, I.; Maillet, D. Mini-and Micro-channels: Influence of Axial Conduction in the Walls, *Int. J. Heat Mass Trans.* **2004**, *47*, 3993.
- (23) Huang, C.Y.; Wu, C.M.; Chen, Y.N.; Liou, T.M. The Experimental Investigation of Axial Heat Conduction Effect on the Heat Transfer Analysis in Microchannel Flow, *Int. J. Heat Mass Trans.* **2014**, *70*, 169.
- (24) De Klerk, A. Adiabatic Laboratory Reactor Design and Verification, *Ind. Eng. Chem. Res.* **2005**, *44*, 9440.
- (25) Schmidt, J.P.; Mickley, H.; Grotch, S. Use of Adiabatic Experiments for Kinetic Studies in Fixed Catalyst Beds, *AIChE J.* **1964**, *10*, 149.
- (26) Aboudheir, A.; Akande, A.; Idem, R.; Dalai, A. Experimental Studies and Comprehensive Reactor Modeling of Hydrogen Production by the Catalytic Reforming of Crude Ethanol in a Packed Bed Tubular Reactor over a Ni/Al<sub>2</sub>O<sub>3</sub> Catalyst, *Int. J. Hydrogen Energy* **2006**, *31*, 752.
- (27) Assabumrungrat, S.; Rienchalanusarn, T.; Praserttham, P.; Goto, S. Theoretical Study of the Application of Porous Membrane Reactor to Oxidative Dehydrogenation of n-butane, *Chem. Eng. J.* **2002**, *85*, 69.

- (28) Qu, W.; Mudawar, I. Experimental and Numerical Study of Pressure Drop and Heat Transfer in a Single-Phase Micro-Channel Heat Sink, *Int. J. Heat Mass Trans.* **2002**, 45 2549.
- (29) Qu, W.; Mudawar, I. Analysis of Three-Dimensional Heat Transfer in Micro-Channel Heat Sinks, *Int. J. Heat Mass Trans.* **2002**, 45, 3973.
- (30) Incropera F.P., DeWitt D.P., Bergman Th. L., Lavine A.S., **2012**, Foundations of Heat Transfer: International Student Version, 6th ed. John Wiley & Sons
- (31) Chatterjee, S.; Degirmenci, V.; Aiouache, F.; Rebrov, E.V. Design of a Radio Frequency Heated Isothermal Micro-Trickle Bed Reactor, *Chem. Eng. J.* **2014**, 243, 225.
- (32) Fernández, J.; Chatterjee, S.; Degirmenci, V.; Rebrov, E.V. Scale-up of an RF Heated Micro Trickle Bed Reactor to a kg/day Production Scale, *Green Proc. Synth.* **2015**, 4, 343.
- (33) Liu, Y.; Cherkasov, N.; Gao, P.; Fernandez, J.; Lees, M.R.; Rebrov E.V., The enhancement of direct amide synthesis reaction rate over  $\text{TiO}_2@SiO_2@NiFe_2O_4$  magnetic catalysts in the continuous flow under radiofrequency heating, *J. Catal* **2017**, in press doi:10.1016/j.jcat.2017.09.010

## Figure captions

- Figure 1. Schematic view of the experimental setup with definitions of reactor dimension and heat transfer parameters.  $r_1=2\text{mm}$ ,  $r_2=3\text{ mm}$ ,  $r_3=6\text{mm}$ .
- Figure 2. Measured (symbols) and calculated (lines) temperatures as a function of the dimensionless reactor coordinate. (a) RF power of 3.1 W, (b) Liquid flow rate:  $160\ \mu\text{L min}^{-1}$ .
- Figure 3. (a) Parity plot for the maximum temperature in the reactor; (b) Parity plot for the position of the maximum temperature in the reactor
- Figure 4. (a) Simulated temperature profiles (lines) vs experimental temperature measurements (points); (b) parity plot obtained at a total input power of 3.1 W at different liquid flow rates.
- Figure 5. Contributions of fluid heating, natural convection and conduction to the overall heat loss in the RF-heated reactor.
- Figure 6. Dimensionless axial position of maximum temperature as a function of M factor.
- Figure 7. Comparison of conversion in the reaction of direct amide bond synthesis in an ideal isothermal reactor and in the RF heated reactor at a reactant flow rate of  $80\ \mu\text{l min}^{-1}$ .
- Figure 8. Synthesis of 4,N-diphenylbutynamide from aniline and 4-phenylbutyric acid.
- Figure 9. The difference in amine conversion between theoretical prediction based on a single point measurement (assuming isothermal conditions) and experimental data.



## Nomenclature

$A_{\perp}$	cross sectional area of the bed, $\text{m}^2$
$A_3$	external surface area of insulation, $\text{m}^2$
$C_p$	liquid specific heat capacity, $\text{J kg}^{-1} \text{K}^{-1}$
$F_V$	volumetric flow rate, $\text{m}^3 \text{s}^{-1}$
$h$	convection heat transfer coefficient, $\text{W m}^{-2} \text{K}^{-1}$
$K$	bed permeability, $\text{m}^{-2}$
$L$	length of reactor, $\text{m}$
$q_V'''$	volumetric heat generation rate, $\text{W m}^{-3}$
$q_{ax}$	axial conduction heat transfer rate, $\text{W}$
$R_A$	conductive thermal resistance in the bed, $\text{K W}^{-1}$
$R_{B1}$	thermal resistance of the reactor wall, $\text{K W}^{-1}$
$R_{B2}$	thermal resistance of insulation, $\text{K W}^{-1}$
$R_{B3}$	thermal resistance of natural convection, $\text{K W}^{-1}$
$T$	temperature, $\text{K}$
$\bar{T}$	average bed temperature, $\text{K}$
$T_{\infty}$	temperature of the surrounding air, $293 \text{ K}$
$U$	overall heat transfer coefficient, $\text{W m}^{-2} \text{K}^{-1}$
$r_1$	inner radius of reactor, $\text{m}$
$r_2$	outer radius of reactor, $\text{m}$
$r_3$	outer radius of insulation, $\text{m}$

Greek symbols:

$\rho$  density of fluid,  $\text{kg m}^{-3}$

$\lambda_1$  effective thermal conductivity of the bed,  $\text{W m}^{-1} \text{K}^{-1}$

$\lambda_2$  thermal conductivity of the wall,  $\text{W m}^{-1} \text{K}^{-1}$

$\lambda_3$  thermal conductivity of insulation,  $\text{W m}^{-1} \text{K}^{-1}$

$\mu$  viscosity,  $\text{kg m}^{-1} \text{s}^{-1}$

$\Phi_{cond}$  axial heat transfer by conduction in the wall,  $\text{W K}^{-1}$

$\Phi_{conv}$  convective heat transfer in the flow,  $\text{W K}^{-1}$

Subscript

*in* inlet

*out* outlet

Table 1. Thermophysical properties of the liquid and solid phase and heat-transfer parameters

Parameter	Value
$U$ [ $\text{W m}^{-2} \text{K}^{-1}$ ]	9.0
$h_3$ [ $\text{W m}^{-2} \text{K}^{-1}$ ]	9.2
$\lambda_{eff}$ [ $\text{W m}^{-1} \text{K}^{-1}$ ]	7.0
$C_p$ , [ $\text{J kg}^{-1} \text{K}^{-1}$ ]	1710
$\rho$ [ $\text{kg m}^{-3}$ ]	861
$T_{inlet}$ [ $^{\circ}\text{C}$ ]	20
$T_{env}$ [ $^{\circ}\text{C}$ ]	20

Table 2. Parameters of fitting functions for temperature profiles at different flow rates

Flow rate	$GC_p$	$R_C^2$	$z_1$	$z_2$	$x_{MAX}^*$
[ $\mu\text{L min}^{-1}$ ]	[ $\text{kg m}^{-2} \text{s}^{-1}$ ]				
40	$6.17 \cdot 10^1$	0.07	0.962	0.742	0.564
80	$1.23 \cdot 10^2$	0.27	1.093	0.653	0.626
120	$1.85 \cdot 10^2$	0.61	1.237	0.577	0.682
160	$2.47 \cdot 10^2$	1.09	1.393	0.513	0.731
200	$3.08 \cdot 10^2$	1.70	1.559	0.458	0.772

Table 3. Parameters of second order polynomial functions  $T(x^*) = ax^{*2} + bx^* + c$  to describe temperature profiles at four different power inputs

Parameter	2.7 W	3.1W	3.4W	3.8W
a [°C]	-207	-241	-272	-291
b [°C]	284	332	378	407
c [°C]	53	57	62	70

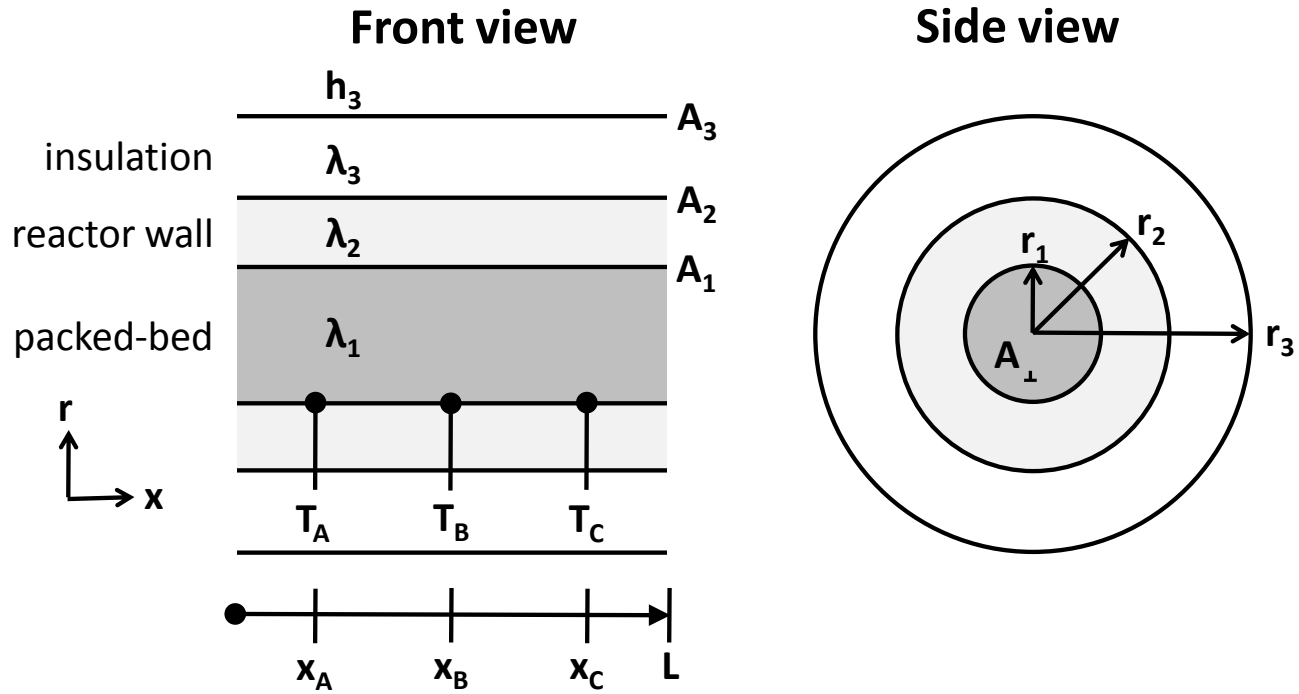
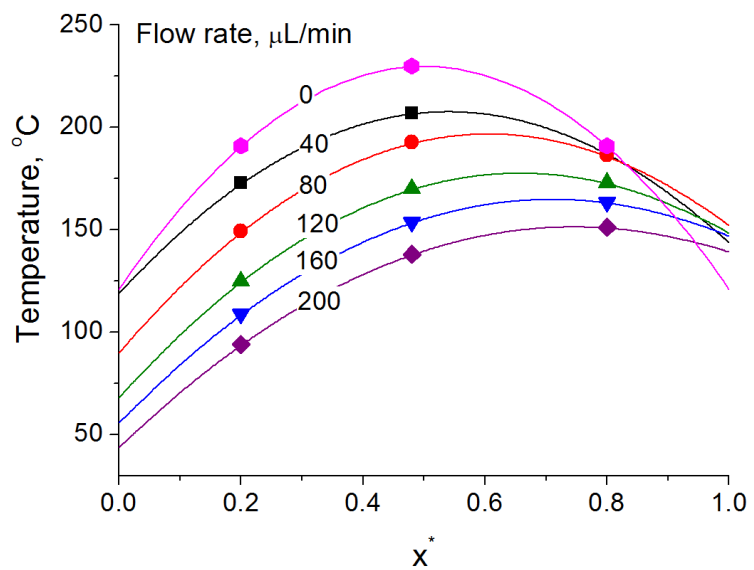


Figure 1

(a)



(b)

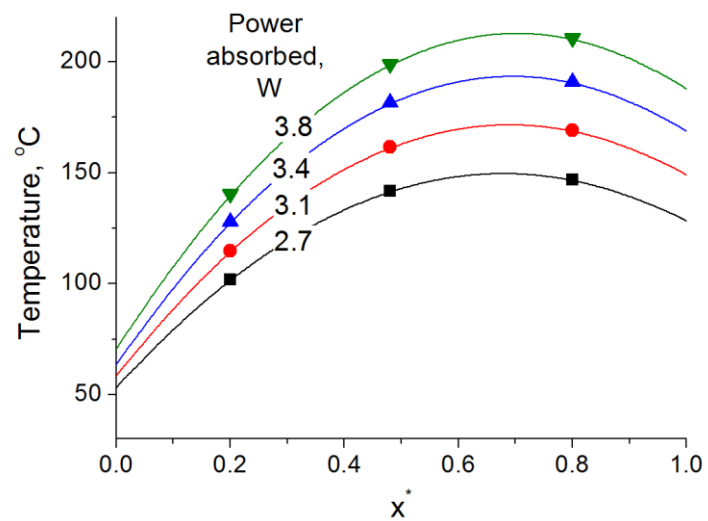
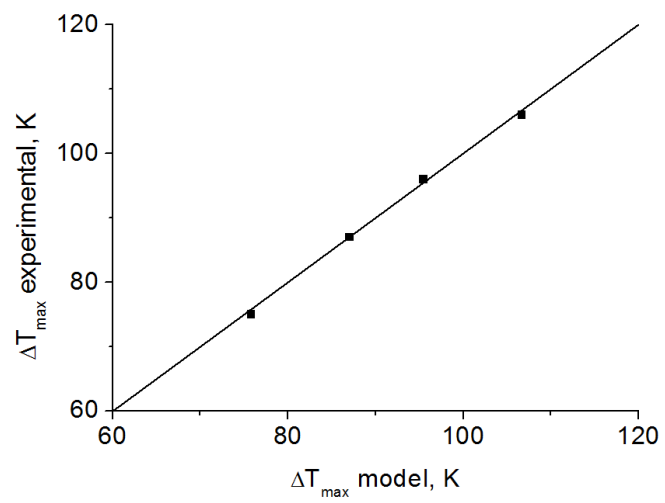


Figure 2

(a)



(b)

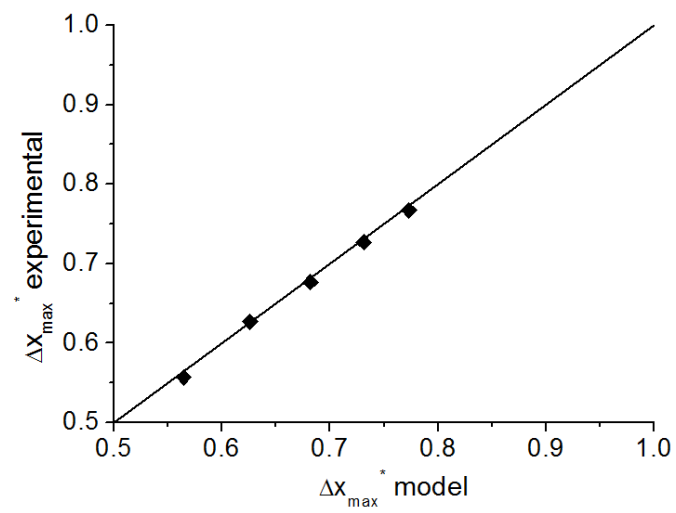


Figure 3

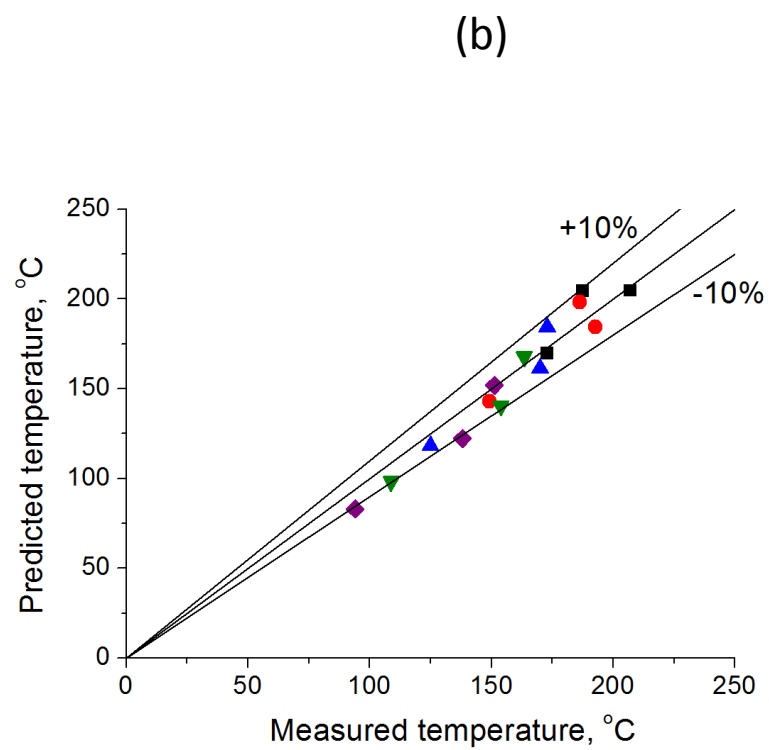
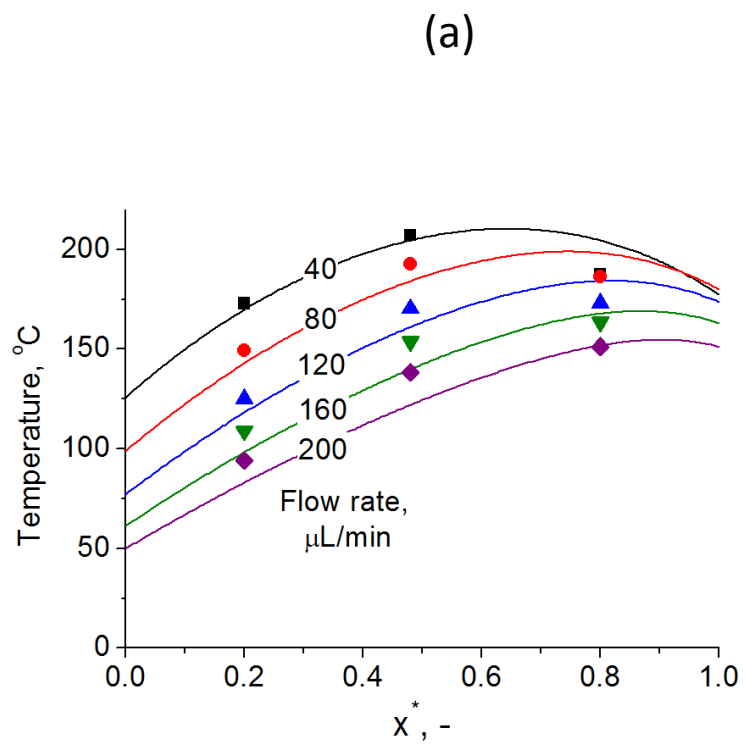


Figure 4



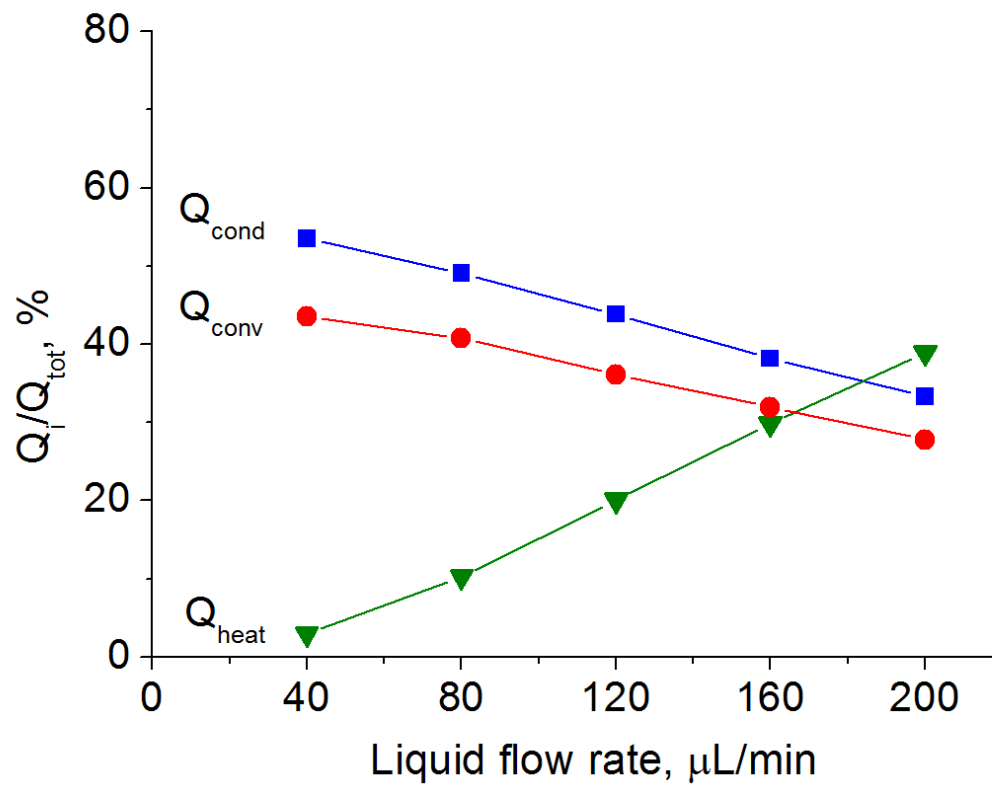


Figure 5

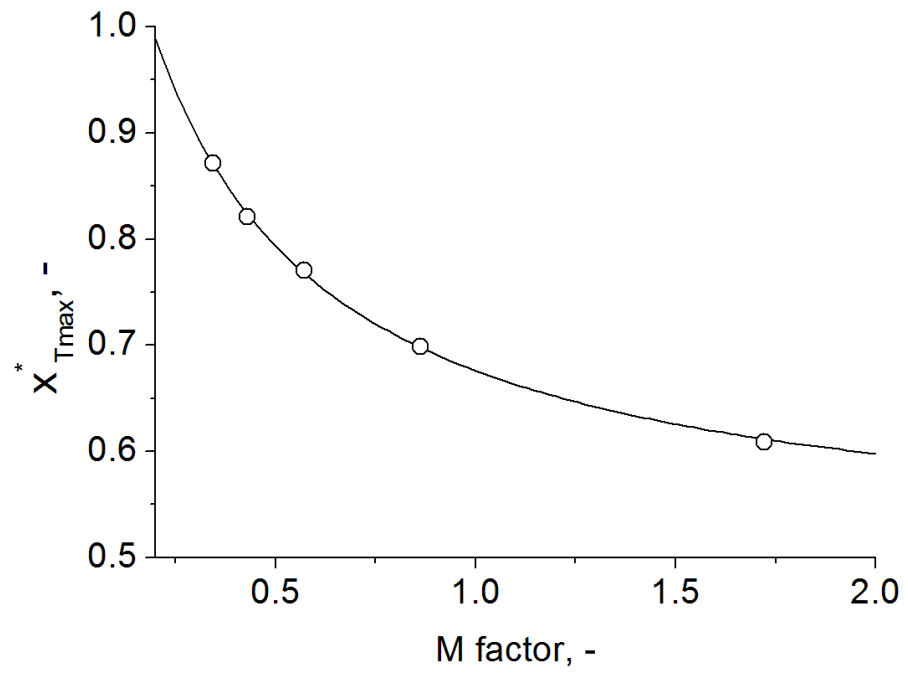
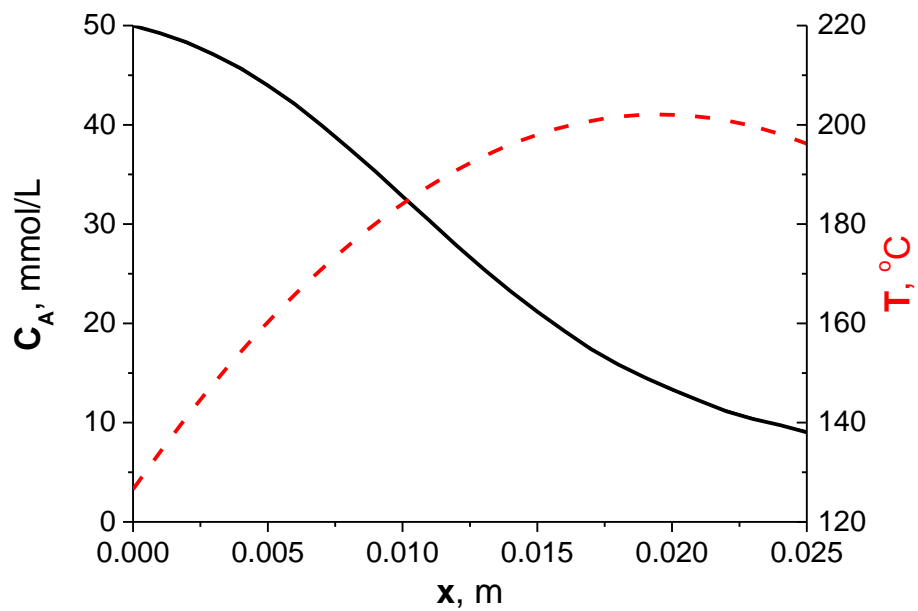


Figure 6

(a)



(b)

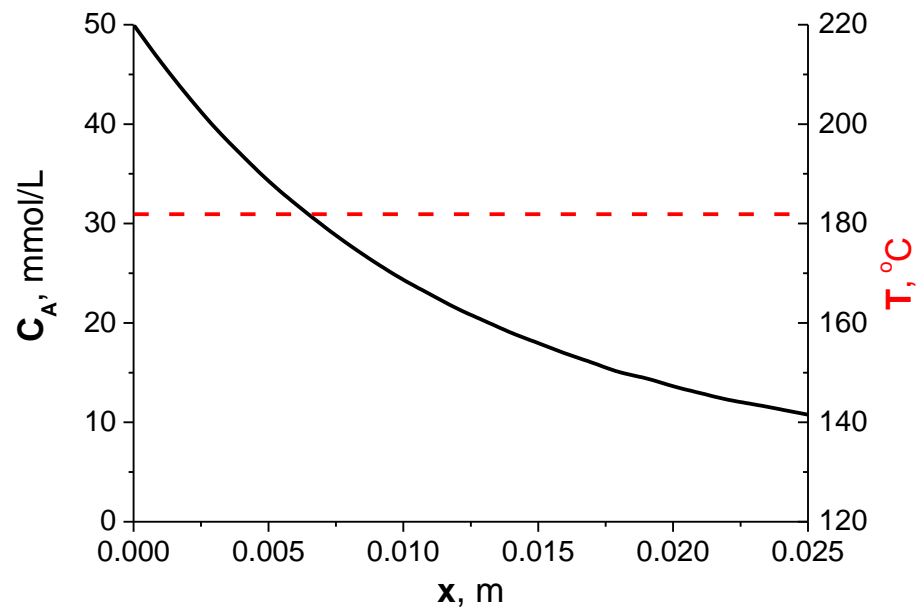


Figure 7

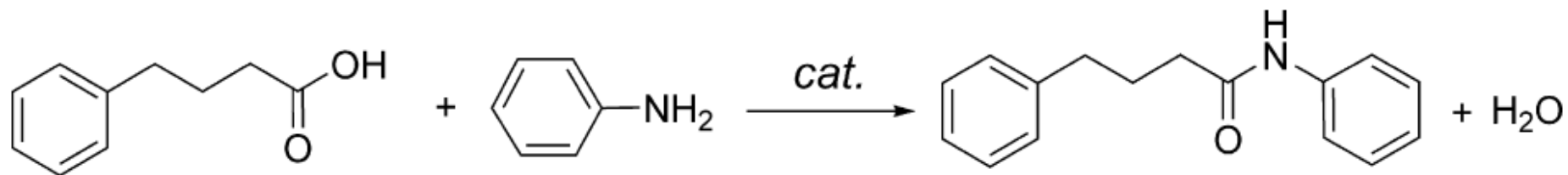


Figure 8

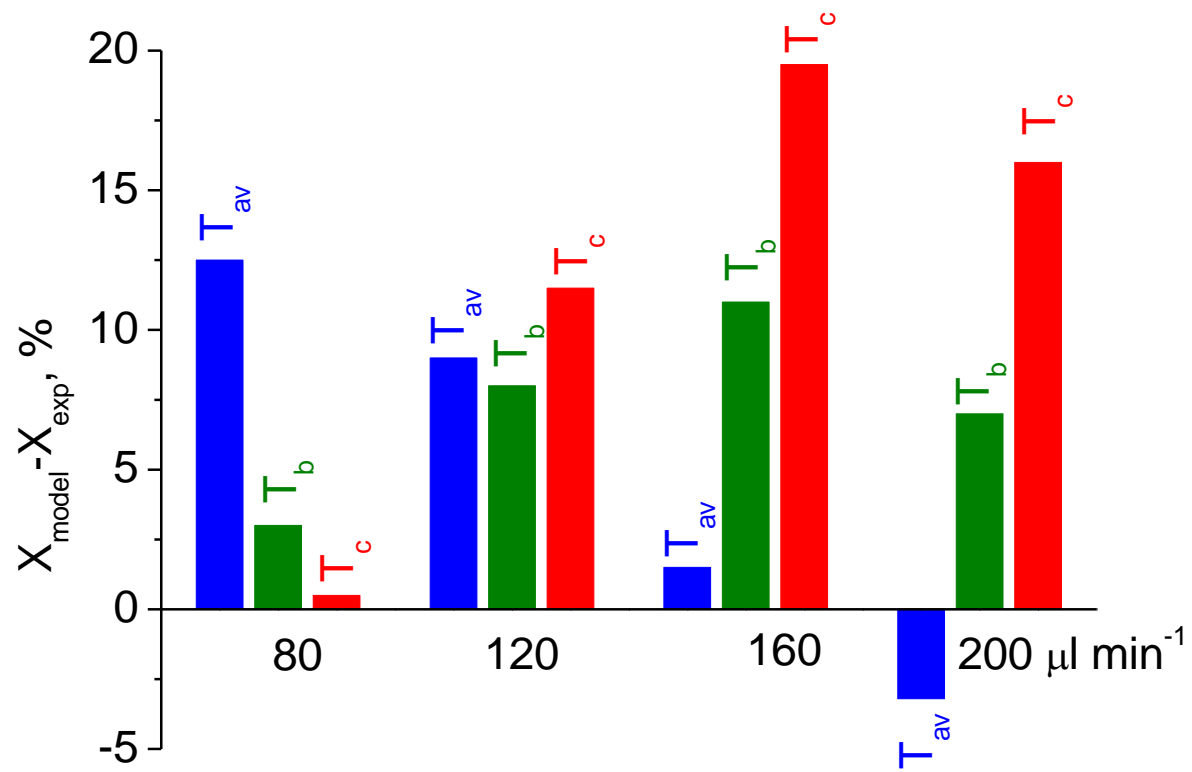


Figure 9